Contents lists available at ScienceDirect

Journal of Power Sources

journal homepage: www.elsevier.com

Review article

Development of cold sintering process and its application in solid-state lithium batteries

Yulong Liu, Qian Sun, Dawei Wang, Keegan Adair, Jianneng Liang, Xueliang Sun*

Department of Mechanical and Materials Engineering, Western University, London, Ontario, N6A 5B9, Canada

ARTICLE INFO

Keywords:
Solid-state battery
Solid-state electrolyte
Cold sintering process
Lithium ion battery
Ionic conductivity
Electrochemical performance

ABSTRACT

Solid-state batteries (SSBs) are developed with the use of inflammable solid-state electrolytes to realize higher energy density and improved safety. However, the densification temperature of solid electrolytes via conventional sintering methods is usually high, especially for oxide-type electrolytes. Advanced sintering techniques such as spark plasma sintering have been developed to decrease the heat-treatment temperature and time. Recently, a novel cold sintering process (CSP) has been developed, which offers an alternative route to the densification of many solid-state electrolyte materials below 300 °C. Generally, the CSP involves multi-stage non-equilibrium processes such as dissolution-precipitation under external stress, viscous flow of saturated solutions and diffusion of species. Herein, the CSP application in different solid electrolytes and electrodes are summarized. It is expected that the CSP has great potential in preparing solid-state batteries with this new sintering technique.

1. Introduction

1.1. History and development of solid-state batteries

Solid-state lithium ion batteries have been considered as one of the most promising next-generation battery systems with improved energy density and safety [1,2]. Among the reported classes of solid-state batteries, bulk-type inorganic solid-state lithium ion batteries show great promise for future EV (electric vehicle) applications. For solid-state electrolytes and solid-state batteries, there has been impressive progress over past decades [3–5]. Herein, we will only give a brief introduction to the development of solid-state electrolytes and batteries.

Generally, oxide electrolytes show good ionic conductivity, chemical stability, and wide electrochemical windows. So, they have received great attentions during past decades. Garnet-type (e.g., $Li_7La_3Zr_2O_{12}$, LLZO) solid electrolyte is one of the most popular investigated oxide-type electrolytes due to its stability against Li metal [6]. Additionally, NASICON-type (e.g., $Li_{1.3}Al_{0.3}Ti_{1.7}(PO_4)_3$, LATP) solid electrolytes have been widely investigated in previous researches due to the high conductivity and availability of raw materials [7]. However, the oxide electrolytes usually need high temperature processing, which makes them difficult to couple with other electrode materials because of side-reactions during co-sintering process. Therefore, soft-electrolytes containing sulfide species have been widely developed. Over the past few years, different sulfide-based systems have been investigated sysmatically [8]. One type of promising sulfide-type electrolyte is Li_2S–P_2S_5 glass-ceramic discovered by Tatsusmisago, it shows a high conductivity close to that of commercial liquid electrolytes due to the precipitation of high conducive crystalline $Li_7P_3S_{11}$ in the matrix [9]. Crystalline sulfides, such as the super ionic $Li_{10}GeP_2S_{12}$ series [10], thio-lithium ion super ionic conductors (thio-LISICON) [11], and argyrodite (Li_6PS_5X, X = Cl, Br, I)-type sulfides were widely studied by different groups after 2010 [12]. Detailed information on inorganic lithium ion con-

* Corresponding author.
Email address: xsun@eng.uwo.ca, xsun9@uwo.ca (X. Sun)

https://doi.org/10.1016/j.jpowsour.2018.05.015
Received 25 March 2018; Received in revised form 2 May 2018; Accepted 4 May 2018
Available online xxx
0378-7753/

ductors can be found in the comprehensive reviews previously reported [13–18].

A monolithic all-solid-state oxide based battery of $Li_4Ti_5O_{12}$/LATP/$LiMn_2O_4$ was fabricated Brike and coworkers, which demonstrated a limited capacity of 40 mAh g^{-1} due to the poor interfacial contact [19]. To reduce the physical mismatch between LATP and electrodes, solid-state batteries were fabricated based on the NASICON electrolytes through deposition of thin film electrodes on the surface of LATP sheets [20–23]. Compared to bulk-type solid-state batteries, the thin-film $LiCoO_2$ electrodes with LATP electrolyte showed an improved electrochemical performance of 120 mAh g^{-1} after annealing, which was attributed to the improved interface between LATP and $LiCoO_2$ electrode.

Ohta and coworkers fabricated a solid battery based on LLZO electrolyte, it showed a limited discharge capacity of 78 mAh g^{-1} due to the large interfacial resistance between $LiCoO_2$/LLZO [24]. Later on, the chemical information at interface between LLZO and $LiCoO_2$ after high temperature sintering was investigated by Park and coworkers, and there was cross-diffusion of Co to LLZO and La/Zr to $LiCoO_2$. In addition, a tetragonal LLZO phase was formed at the interface due to the leaching of Al at high temperature, which further decreased the ionic conductivity at interface [25].

Furthermore, the moisture and carbon dioxide sensitivity of LLZO in the ambient environment has been proven to be problematic for bulk-type solid-state batteries with LLZO electrolyte, which may be unstable after assembly in air [26]. To reduce the influence of Li_2CO_3 and in-homogenous contact at the electrode-electrolyte interface, different strategies such as co-sintering and the insertion of buffer layers were adopted for garnet-type electrolyte interfaces. As an example, Li_3BO_3 (LBO) has been used as a sintering additive to reduce the heating temperature for the fabrication of LLZO/LCO cells at a lower temperature of 700 °C [27]. With the addition of Li_3BO_3 and Al_2O_3, co-sintering of Al-doped LLZO/LCO was successfully prepared due to simultaneous inter-diffusion of Al between garnet oxide and additives, which delivered a charge-discharge capacities of 98 and 78 mAh g^{-1}, respectively [28].The formation of a stable and ionically conductive interface between solid electrolyte and electrode is critical to achieving functional solid-state batteries. To alleviate the influence of Li_2CO_3, Li and coworkers proposed that the incorporation of a small amount LiF into the garnet LLZO electrolyte could effectively decrease the interface resistance from 1260 Ω cm^{-2} to 345 Ω cm^{-2} [29]. As an alternative strategy to form a stable interface, Han and coworkers utilized the Li_2CO_3 layer on LLZO by forming a highly conductive Li_2CO_3-Li_3BO_3 glass-ceramic buffer layer to reduce the interface resistance between LLZO and $LiCoO_2$. The full cell was capable of delivering a discharge capacity of 120 mAh g^{-1} at 100 °C and a long cycling life of over 100 cycle at room temperature [31].

To further reduce the solid-state diffusion length between electrode and electrolyte, 3D porous scaffold solid electrolytes were invented. The electrode materials were filled into the pores using a wet chemical method followed by heat treatment, which resulted in lower sintering temperatures and good electrolyte/electrode contact, as illustrated by Kotobuki and coworkers [32,33]. Until now, the oxide-based solid-state electrolytes have faced significant challenges in interfacial contact and conductivity, and further efforts in both materials design and novel fabrication processes are required to make further advancements.

Unlike the rigid mechanical properties of oxide-based electrolytes, the sulfide glass-type electrolytes are soft and have higher ionic conductivities. Therefore, the interfacial problems can be easily addressed through high-pressure pressing at room temperature through room-temperature sintering mechanism. For example, Li_3PO_4-Li_2S-SiS_2 glass electrolyte was pressed with spherical graphite and TiS_2 in a full battery. The overall resistance of fabricated cell was close to the resistance of pure solid electrolyte layer, which indicated that the interfacial contact resistance was negligible. Another example was the Li_2S–P_2S_5 glass-ceramic electrolyte, it was used in the fabrication of solid-state batteries with $LiCoO_2$ cathodes by Ohta and coworkers. A capacity of 102 mAh g^{-1} at room temperature was delivered, which was 73% of theoretical capacity of $LiCoO_2$ [36]. To increase the performance, a highly conductive Li_2S–P_2S_5–GeS_2 (thio-LISICON) sulfide electrolyte was prepared by Kanno and coworkers, where the as-prepared In/thio-LISICON/$LiCoO_2$ discharge capacity was only 80 mAh g^{-1} due to reduction of Ge species [37]. In order to stabilize the interface and reduce the side reactions, argyrodite-type sulfide Li_6PS_5X(X = Cl, Br, F, I) electrolyte was recently developed and applied in solid-state batteries due to its high electrochemical stability. Yubuchi and coworkers synthesized argyrodite sulfide electrolytes using a solution method followed by the fabrication of cells with a Li-In alloy anode and $LiNi_{1/3}Mn_{1/3}Co_{1/3}O_2$ (NMC) layered cathode, showing a capacity of 140 mAh g^{-1} at room temperature [38]. Discovered in 2011, a superionic conducting $Li_{10}GeP_2S_{12}$ demonstrated an extremely high ionic conductivity of 1×10^{-2} S cm^{-1} [10]. In 2016, the same group fabricated batteries using this new superionic conductor with higher chemical stability, which showed a stable cycling performance for 1000 cycles [39]. Compared to oxide based solid-state batteries, sulfide based solid-batteries shows better electrochemical performance due to the low interfacial resistance.

Bulk inorganic solid-state batteries have achieved remarkable progress in recent years. Nevertheless, there are still several major challenges that need to be addressed in order to realize their practical application. The problems that need to be overcome include the synthesis of a robust solid electrolyte with high ionic conductivity, poor interfacial compatibility and stability, and low-cost cell fabrication processes. Among the prominent interfacial problems, the severe side reactions between solid-state electrolyte and electrode during high-temperature sintering has largely impeded the progress of solid-state lithium ion batteries. Formation of an ion-blocking interface will increase the interface resistance and slow down the transport of lithium ions. Therefore, the next section will address this issue with the development of advanced sintering techniques.

1.2. Development of sintering techniques for solid-state batteries

Solid electrolyte particles need to be bonded together by sintering before use in batteries. A sintering process usually involves two major steps: densification and grain growth. Both steps require a thermodynamic driving force, that is, the reduction of the total Gibbs free energy of the system, rendering them thermodynamic favorable. Therefore, the process of sintering is intrinsically driven by the Gibbs free energy.

During the sintering process, two popular mechanisms are often mentioned in literature: solid-state sintering and liquid phase sintering [40]. The latter is preferred during solid elec-

trolyte preparation because of the simplicity and effectiveness in reducing the sintering temperature. The so-called liquid phase sintering is a process where liquid-phases emerge during the sintering process, which is beneficial for mass transport and particle compaction. The typical process of liquid phase sintering is divided into multiple stages. The initial stage is similar to solid-state sintering, wherein the particles are bonded together with the help of a liquid-phase formed at high temperature. The second stage involves the crystallization of dissolved species after the liquid-solution is over-saturated. The final stage is the mass transport process, which result in the exchange of atoms between different particles and finally grain growth [41].

Conventionally, the sintering of materials only involves the application of heat upon a green body with 40–60% density, which can facilitate the mass transport/diffusion. Thus, some advanced sintering techniques are developed by utilizing other factors such as external pressure and/or electric field in combination with external heating to facilitate the mass transport. Caused by pressure or an applied electric field, the mass transport in materials can be largely enhanced, and lower sintering temperatures can be realized. Several advanced sintering techniques that are widely reported in the densification of solid electrolytes include hot pressing, field-assisted sintering, flash sintering, microwave sintering and spark plasma sintering. Here, we will briefly introduce the basic principles of the advanced sintering techniques and list some examples for further understanding [41,42].

Hot pressing is a sintering technique based on the stress-intensity densification mechanism. The mass transfer/diffusion between particles is accelerated during the sintering process due to the pressure gradient created by the external force applied on particles, thereby decreasing the sintering temperature and time. By hot-press sintering of the screen-printed electrodes on the as-sintered electrolyte pellet, Kobayashi and coworkers fabricated a $Li_3V_2(PO_4)_3/Li_{1.5}Al_{0.5}Ge_{1.5}(PO_4)_3/Li_3V_2(PO_4)_3$ symmetric battery (LVP as both cathode and anode). This process was able to avoid the electrolyte/electrode element mutual-diffusion phenomenon, and no impurity phases were observed in the sintered sample [21]. The as-obtained battery delivered a discharge specific capacity of 104 mAh g^{-1} at 80 °C and 42 mAh g^{-1} at 25 °C, respectively. Furthermore, as reported by Sakamoto and coworkers, an ionic conductivity of 4.0×10^{-4} S cm^{-1} was observed at room temperature for the hot-pressed $Li_7La_3Zr_2O_{12}$ (LLZO) pellet at 1000 °C with 40 MPa pressure [43]. To increase the ionic conductivity of the electrolyte, this group introduced some doping elements at different atomic sites to stabilize the cubic crystal structure of the LLZO pellet. An ionic conductivity of 8.7×10^{-4} S cm^{-1} at room temperature was obtained after hot-pressing for Ta doping LLZO [44]. Apart from the oxide solid electrolytes, hot-press sintering was widely used in sulfide electrolytes as well, especially for glass-ceramic sulfides (Li_2S-P_2S_5) [45].

Field-assisted sintering is widely used for ceramics, especially for low or non-conductive materials. The working principle behind this method is the passing of heat through a graphite die under high-current in short time [46]. [47] The application of field-assisted sintering was proven to be effective in the preparation of oxide solid-state electrolytes in previous reports. Zhang and coworker applied this technique in the synthesis of LLZO electrolyte for the first time [48]. They showed that LLZO could be densified from 1100 to 1180 °C within 10 min, and a high conductivity of 5.7×10^{-4} S cm^{-1} at room was obtained with a maximum relative density of 99.8%. By using a novel wet-chemical method to prepare the nano-sized LLZO precursors, the sintering temperature of LLZO electrolyte was further lowered down to 1000 °C, and a relative density of 96.5% was achieved [49]. In a separate study, Rosenberger conducted experiments on LATP ($Li_{1.3}Al_{0.3}Ti_{1.7}(PO_4)_3$) electrolyte with field-assisted sintering [50]. It was shown that the relative density could be drastically improved from 85% at 0 V to 95.5% at 20 V, however, a high resistance was obtained when sintering at increased voltages. The reason behind the increased resistance is the poor intergranular contact and high grain-boundary resistance between large-grains. Furthermore, with a modified sol-gel method, Hoffman and coworkers succeeded in the densification of LATP electrolyte in the temperature range of 850–1000 °C [51]. For LATP with a pure phase composition, a relative density of 98% was obtained, which can achieve a high conductivity of 10^{-3} S cm^{-1} at room temperature.

Flash-sintering is similar to field-assisted sintering, except the applied current is alternative current [52]. In flashing sintering, there is a possibility of lithium loss due to crystal structure breakdown, which makes the technique unsuitable for densification of solid electrolytes. Stoldt and coworkers applied flash sintering on a LAGP ($Li_{1.5}Al_{0.5}Ge_{1.5}(PO_4)_3$) electrolyte with a high frequency electric field. While no such deterioration behavior was observed due to the use of high frequency, the pellet demonstrated an ionic conductivity of 1.5×10^{-4} S cm^{-1} [53]. This work demonstrated the ability of electric field sintering in condensing conductive electrolytes with high frequency.

Similar to the pressure effects that can enhance sintering, the application of an external field such as electromagnetic radiation can improve the sintering process [41]. Microwaves can also be utilized as the heat sources in the sintering process, especially for high dielectric ceramics such as solid electrolytes [54]. Perovskite-type (LLTO, $La_{0.5}Li_{0.5}TiO_3$) electrolytes are usually sintered at high temperature, which leads to lithium loss. As an alternative, Nan and coworkers prepared LLTO by a microwave sintering method [55]. A dense LLTO ceramic was obtained, and exhibited a different lattice structure and microstructure in comparison with the conventional sintering method. Unfortunately, a lower ionic conductivity (7.2×10^{-7} S cm^{-1}) was obtained due to the formation of more grain boundaries.

During spark plasma sintering (SPS), an electric current is pulsed through a conductive die, such as graphite, to apply thermal energy on powders through Joule heating [56]. Near theoretical sinter-densities can be achieved with significantly shorter holding time for any powder compacts, regardless of the electrical conductivity of the powders [56,57]. In the past years, tremendous efforts have been dedicated to fabricating dense solid electrolytes and solid-state batteries using spark plasma sintering. Different solid electrolytes, such as perovskite LLTO, NASICON-type Y doped $LiZr_2$ $(PO4)_3$, and garnet LLZO electrolyte were prepared using the spark plasma sintering technique [58–61]. In addition, cathode materials including $LiFePO_4$, Li_2CoPO_4F, and $LiCoO_2$, were densified as well [62–64]. Aboulaich and coworkers fabricated a Li_3V_2 $(PO_4)_3/Li_{1.5}Al_{0.5}Ge_{1.5}$ $(PO_4)_3/LiFePO_4$ solid-state battery, which delivered a capacity of 80 mAh g^{-1} at 0.05 C rate [65]. Furthermore, Kobayashi and coworkers recently assembled a solid-state battery with $LiCoO_2$ electrode and a new $Li_{2.2}C_{0.8}B_{0.2}O_3$ oxide-electrolyte that was capable of deliver-

ing a discharge capacity of 118 mAh g^{-1} at 10 μA cm^{-2} [66,67].

In this section, we illustrate that the sintering temperature and time of solid electrolyte/battery materials can be well-controlled through a combination of applied pressure, temperature and electric field using different sintering techniques (Table 1). However, a temperature of 600–1000 °C is still high enough for side reactions to occur between electrode and electrolytes. In the following section, we introduce a novel sintering process which can enable sintering of solid electrolyte/battery materials at a temperature less than 300 °C.

2. Basics of the cold sintering process

2.1. Background of the cold sintering process

The term cold sintering was firstly introduced in 1978 by Gutamanas and coworkers [68]. It was named as cold sintering because the metal/ceramic powers were compacted at a high pressure (~GPa) and relative low temperature, such processes were widely observed in power metallurgy field.

In 1986, a hydrothermal assisted hot pressing concept was generated by combining hydrothermal processing with isostatic pressing, and a broad series of ceramics were prepared with more than 90% theoretical density [69]. For instances, nanometric α-quartz was successfully densified at low temperature with sol-gel silica as precursors. The underlying mechanism shows that water as an additive plays an important role in the densification process through forming the inter-particle necks [70,71]. Very recently, researchers reported the densification of precursors of $BaTiO_3$ ceramic with a new process of reactive hydrothermal process at low temperature [72].

Inspired by these previous works, a new type of CSP for ceramics was invented by Randel's group [73–75]. The new CSP can enhance the inter-diffusion between particles through adding a transient solvent to the powder, which enables low temperatures (120 ℃-300 °C) and pressures (350–500 MPa) during the sintering process, unlike the traditional cold sintering with high pressure.

2.2. Typical stages of the cold sintering process

The CSP can be described at the macro- and micro-levels, as depicted in Fig. 1 [75,76]. As shown in Fig. 1a, a liquid phase is introduced at the particle-particle interface and the particle ensembles are homogenously wetted with an appropriate amount of solution (water or volatile solutes). The powders are then compacted under an external pressure, which is facilitated by the addition of liquid lubricant at the particle interfaces. Furthermore, the sharp edges of the particles are dissolved into the solution and then precipitate into pores or interstitial spaces between particles under an applied external pressure and heat. Finally, the powders are sintered together after the complete removal of the solution [76].

From the microstructure observations collected in previous reports, the CSP can also be described as in Fig. 1b, which involves the dissolution and rearrangement of atoms at the surface sites of crystals after wetting of the surface. This is followed by a dissolution-precipitation process, which is triggered by the breakdown of an equilibrium state of solid-liquid mixture phases. In this stage, ionic species and/or atomic clusters diffuse through the liquid and precipitate on particles at sites away from the stressed contact areas. Finally, an amorphous phase may form in the grain boundary regions after sintering, leading to suppressed grain boundary diffusion or mobility and thus limited grain growth [75].

During the CSP, three possible mechanisms are proposed to enable enhanced particle compaction and mass transport, including liquid-enhanced creep, Marangoni flow at the liquid-liquid interphase and diffusiophoresis at the solid-liquid interface. It can be concluded that the CSP process is an outcome of multiple mechanical-chemical coupling effects, which yields improved mass transport and is further beneficial for the particle densification process [76].

Table 1
Summary of sintering techniques for solid-state batteries.

Sintering technique	Solid Electrolyte/Solid Battery	Sintering parameter	Performance	Ref.
Hot sintering	LLZO	1000 °C/1 h, 40 MPa, 98%	4.0×10^{-4} S cm^{-1}	[43]
Hot sintering	Ta-LLZO	1000 °C/1 h, 40 MPa, 98%	8.7×10^{-4} S cm^{-1}	[44]
Field assisted sintering	Al-LLZO	1150 °C/3 min, 10 MPa, 99.8%	5.7×10^{-4} S cm^{-1}	[47]
Field assisted sintering	LATP	900 °C/3 h, N/A, 95.5%	~1×10^{-3} S cm^{-1}	[51]
Flash sintering	LAGP	800 °C/1 h, N/A, N/A	1.5×10^{-4} S cm^{-1}	[53]
Microwave sintering	LLTO	800 W/20 min N/A, 97%	7.2×10^{-7} S cm^{-1}	[55]
Spark plasma sintering	NASICON (Y-doped LZP)	1200 °C/20 min, 40 MPa, 90%	1.4×10^{-4} S cm^{-1}	[58]
Spark plasma sintering	LLZO	1000 °C/10 min, 50 MPa, N/A	1.3×10^{-4} S cm^{-1}	[59]
Hot sintering	$Li_3V_2(PO4)_3$/LAGP/$Li_3V_2(PO_4)_3$	840 °C/2 h, 49 MPa, N/A	104 mAh g^{-1} (80 °C) 42 mAh g^{-1} (25 °C)	[22]
Spark plasma sintering	$Li_3V_2(PO_4)_3$/LAGP/$LiFePO_4$	680 °C/2 min, 100 MPa, N/A	80 mAh g^{-1}	[64]
Spark plasma sintering	$LiCoO_2$/$Li_{2.2}C_{0.8}B_{0.2}O_3$/Li	450 °C/1 min, 30 MPa, N/A	118 mAh g^{-1}	[65]

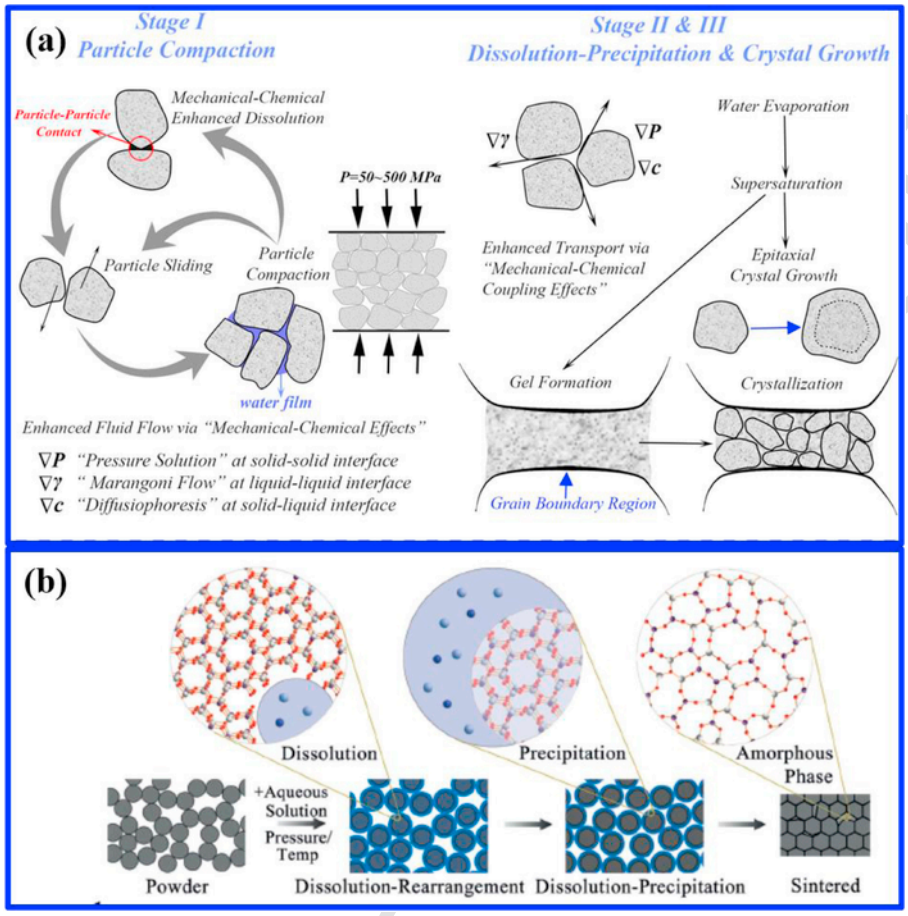

Fig. 1. Principles and process of cold sintering; (a) the three stages of the cold sintering process, and (b) the mechanism of cold sintering at the micro-structure level [75,76].

2.3. Factors affecting the cold sintering process

As investigated by Clive's group, the CSP process is determined by several physical/chemical factors such as the choice of starting materials, solute and physical parameters [77–80]. The most important step is establishing a proper solution system that can enable an environment for the chemical reactions to take place. Due to the nature of material dissolution, three different situations were observed experimentally [73]. (1) In the case of the congruent dissolution of materials, especially hygroscopic compounds, the CSP is relatively simple and proceeds through a direct method. (2) If the materials are incongruent dissolution, for example, $BaTiO_3$, a passivating surface appears on the surface that prevents the precipitation process and further densification [81]. To solve this issue, a saturated solution at the required stoichiometric ratios is introduced to enable particle rearrangement, growth, and therefore densification. (3) For materials with negligible dissolution, a similar strategy is adopted through intentionally creating an aqueous solution that contains the corresponding chemical constituents [82].

Compared to the conventional sintering processes, the CSP can occur within a relatively low temperature region, as shown in Fig. 2a [81]. Taking $BaTiO_3$ as an example, the CSP region lies in the range of 120–900 °C, while the temperature of conventional sintering or advanced sintering techniques are 100–300 °C higher than that of the CSP. As illustrated in Fig. 2b, the requirements of Gibbs free energy reduction in the CSP is less compared to that in conventional sintering routes due to the smaller energy barrier, which accounts for the lower sintering temperature of the CSP [76]. This low-temperature behavior originates from the unique processing pathway and special dynamic environment. In contrast to traditional sintering techniques, the CSP is performed in a multistep manner. In each step, the free energy barrier is relatively lower and could be easily overcome with the assistance of various mechanical-chemical effects. The Gibbs energy change of the CSP is greatly reduced due to the combination of liquid-assisted particle sliding and hydrothermal-assisted sintering procedures. In addition, the traditional sintering methods need to overcome a huge energy barrier between the initial particles and final consolidation status. The CSP phenomenon is similar to some natural sintering examples such as the formation of rocks and generation of pearl. In contrast, the production of poly-crystals by solid-state reaction is more difficult in industry.

2.4. Proposed mechanism of the cold sintering process

The use of the CSP has been reported with a wide range of ceramic and polymeric materials [79]. However, an understanding of the underlying mechanism of the CSP is still unclear. Based on the previous results, a unique mechanism of the cold sintering process was proposed by Clive's group, as shown in Fig. 3 [80].

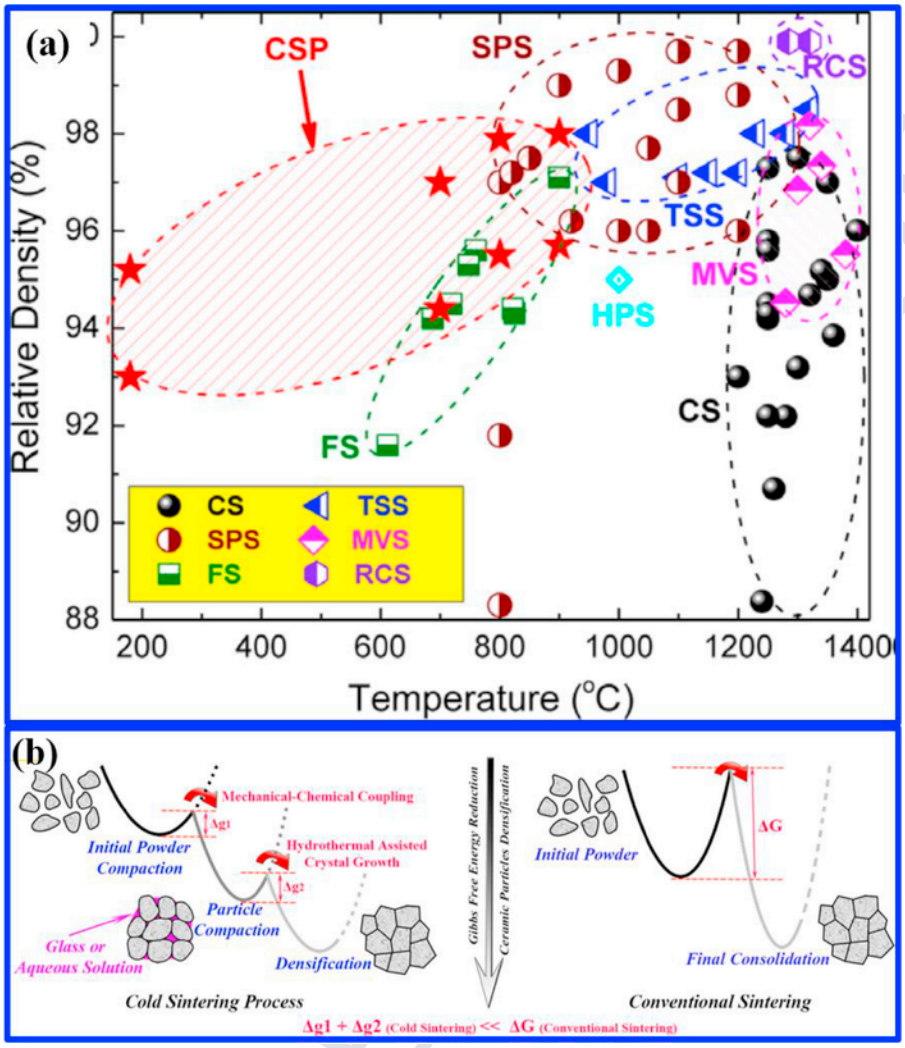

Fig. 2. The cold sintering process at low temperature; (a) The relative density of cold sintered materials in comparison with other sintering techniques, and (b) schematic diagram showing the Gibbs free energy change during cold sintering [76]. [81].

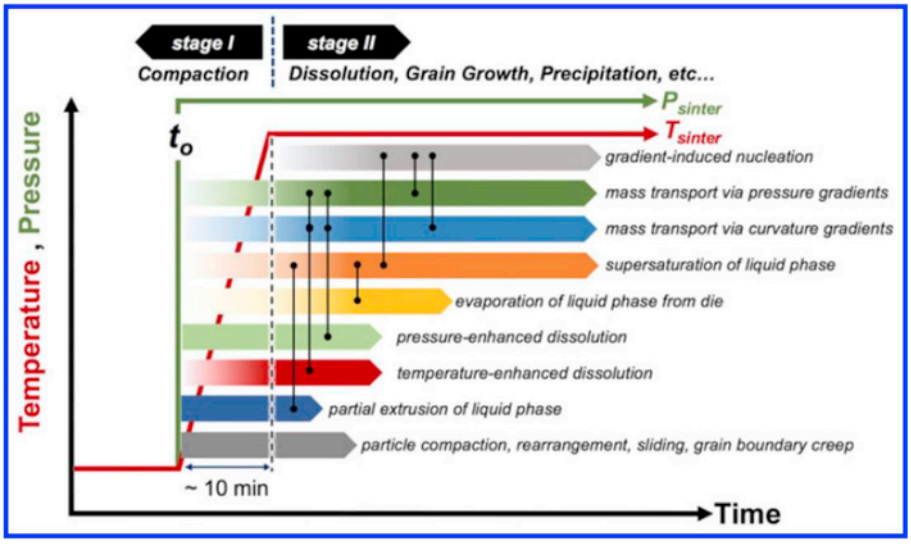

Fig. 3. Proposed mechanism of cold sintering process [80].

The first step is the densification stage, that is, the compaction of loosely-packed powders with the assistance of a liquid phase. As indicated by the proposed mechanism, the step involves particle rearrangement, sliding of powders under fluid mechanics, and grain boundary creep. In addition, the edges of particles are dissolved with the help of pressure and temperature gradients during the compaction stage. At the same time, excess liquid escapes from the pellet-press due to the poor sealing. Afterwards, the liquid phase is saturated with the evaporation of the solvent, and the precipitation process begins. Meanwhile, the mass transport is enhanced under the influence of pressure and curvature gradients at the grain-boundaries. Finally, the crystals begin to nucleate at the grain boundaries and surface of the highly hydroscopic materials after the evaporation of the liquid. The importance of this process was highlighted by Sebastian et al. in the preparation of a dielectric Al_2O_3-NaCl composite with a relative density of 96%, where such a high relative density is achieved due to the hydroscopic nature of NaCl [83]. However, in many cases there is the formation of intermediate phases between grains, as observed experimentally [79].

In a recent report by Guillon and co-workers on the CSP of ZnO with a small amount of water, they argued that the solution-precipitation mechanism proposed by Randall group was not enough to activate the densification process. Due to the diffusion of H^+ and OH^- ions into the ZnO crystal, a high defect concentration could be produced at the grain boundaries with high potentials. Because of the formed defect sites, a high diffusion path was created, which was beneficial for mass-transport and low-temperature sintering. In the case of zinc acetate as additive, larger crystal growth could be promoted along the preferred crystallographic planes due to the change of ionic species concentration at surface of ZnO [84]. The water could also trigger the flash sintering process at low temperature by increasing the specimen conductivity, as observed by Luo et al., which extended the idea of CSP to field of water-assisted flash sintering process [85].

Recently, a new assumption was proposed by Chen et al. by comparing the mechanical behavior of dry and cold-sintered NaCl. The dry-pressed NaCl showed lower relative density than the cold sintered NaCl at low applied pressure where dissolution-precipitation process dominated. In high applied pressure of 200–300 MPa region, mechanical deformation became prominent in densifying the NaCl powders. Due to the low hardness of the NaCl crystal, the particles could be easily rearranged and reshaped by mechanical force. Thus, the plastic deformation for NaCl CSP cannot be neglected, especially at high applied pressure [86].

Although there have been some reports on the CSP of inorganic compounds, the process is still at a very early stage. The best way to gain further understanding of the mechanism of the CSP is to develop more materials in this field. There are several opportunities awaiting in the future for expanding and deepening our comprehensive understanding of this process.

3. The development of cold sintering processes for solid-state batteries

3.1. Cold sintering of solid-state electrolytes

For solid-state electrolytes, the transport of lithium ions is usually slow at the highly-resistive grain boundaries. To minimize the effect of the grain boundary on the ionic conductivity of the electrolyte, high-temperature treatment is required to enhance the interconnectivity between grains. However, high-temperature sintering has two detrimental side-effects, i.e., lithium loss and secondary phase formation. To counteract the lithium loss, advanced sintering techniques such as spark plasma sintering have been developed. However, the temperature range of spark plasma sintering still possess the chance of side-reactions and requires a complicated manufacturing process, making it hard to scale up.

Usually, the densification of sulfide-type electrolytes was more attainable due to its low modulus, even at room temperature. This process was exemplified by Tatsumisago et al., who proposed a room temperature pressure-sintering mechanism for sulfide electrolytes [87]. They ascribed the room temperature sintering to the low bond energies between the cation and anion species of the sulfide materials, which resulted in small-scale plasticity, making them favorable for room temperature sintering. Following this discovery, cold pressing was widely adopted for the processing of sulfide-based solid electrolytes (Table 2). However, the oxide-type electrolytes still require a high-temperature treatment to facilitate the mass-transport between particles. Only after high temperature sintering will the oxide solid electrolyte exhibit a high conductivity because of the drastic reduction of grain-boundary resistance.

Recently, LAGP ($Li_{1.5}Al_{0.5}Ge_{1.5}(PO_4)_3$) solid electrolyte was prepared with the CSP method for first time by Seth et al. [92] By adding ethanol or water as the solvent during the CSP process, LAGP pellet with a density of 80% was achieved at 120 °C in 20 min. However, the pellet showed a relatively low ionic conductivity at room temperature due to the formation of an amorphous phase at the grain boundaries. After annealing at 650 °C (the crystallization temperature of LAGP), the ionic conductivity of the LAGP pellet reached up to 5.4×10^{-5} S cm^{-1} at room temperature (as shown in Fig. 4a). From the EIS tests, it was seen that the improvement in ionic conductivity was attributed to the re-crystallization of amorphous surfaces in the CSP sintered LAGP. Nonetheless, they did not offer the microstructure evidence to prove the re-crystallization phenomenon at the grain boundary of LAGP.

In addition to the traditional LAGP solid electrolyte, composite systems such as LAGP/(PVDF-HFP) have been fabricated by the CSP process at 120 °C with water as the solvent (as

Table 2
Summary of low-temperature sintering of solid electrolytes.

Solid Electrolyte	Sintering parameter	Young's moduli	Performance	Ref.
$25Li_2S{\cdot}75P_2S_5$ glass	RT/260Mpa	18 GPa	3.0×10^{-4} S cm^{-1}	[88]
$70Li_2S{\cdot}30P_2S_5$ ($Li_7P_3S_{11}$) glass	RT/360Mpa	22 GPa	1×10^{-3} S cm^{-1}	[88]
$90Li_3BO_3{\cdot}10Li_2SO_4$	RT/360Mpa	53 GPa	9.4×10^{-6} S cm^{-1}	[89]
$33Li_3BO_3{\cdot}33Li_2SO_4{\cdot}33Li_2CO_3$	RT/360Mpa	51 GPa	1×10^{-5} S cm^{-1}	[90]
NASICON + LiTFSI salt	120 °C/450Mpa	139 GPa	5×10^{-5} S cm^{-1}	[91]

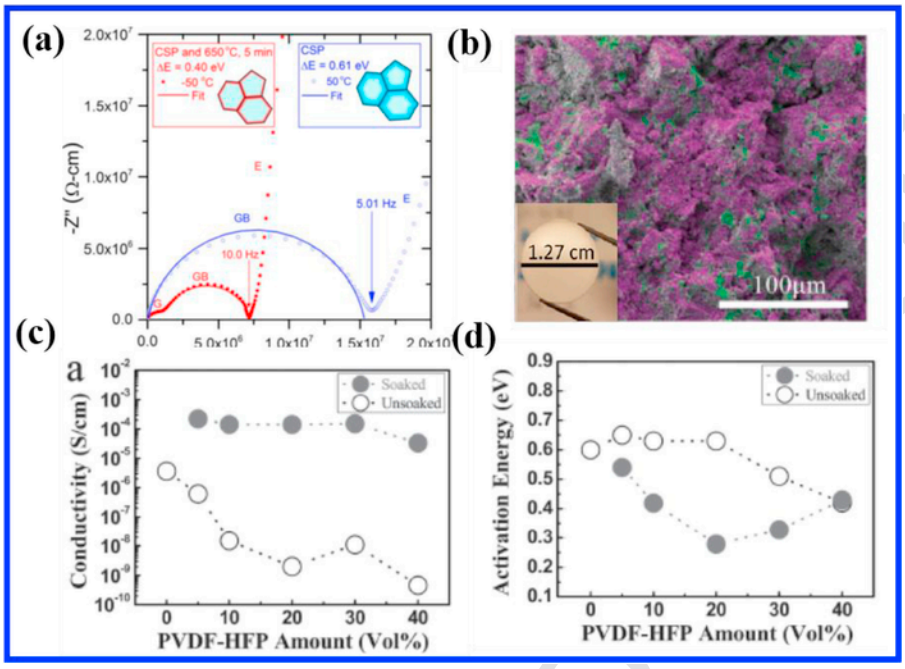

Fig. 4. Cold sintering of LAGP electrolyte; (a) EIS of LAGP before and after annealing, (b) EDS mapping of LAGP/PVDF-HFP composite, (c) conductivity of the composites, and (d) activation energy of composites [74]. [92].

shown in Fig. 4b–d) [74]. Due to the low ionic conductivity of the PVDF-HFP polymer, the conductivity of the composite electrolyte was found to decrease with an increase of polymer content. However, after soaking in a liquid electrolyte, the conductivity was increased due to the formation of fast ion transportation pathways through liquid electrolyte. In the report, with 5–10 wt % liquid electrolyte, the room temperature ionic conductivity could increase to 1.0×10^{-4} S cm^{-1} at room temperature (as shown in Fig. 4c) [74]. At the same time, the activation energy for the ionic conductivity was drastically reduced compared to the pellet without soaking in liquid electrolyte. The relative density of the LAGP/(PVDF-HFP) composite was found to be close to 86%, which was significantly higher than the dry-press pellet without the addition of solvent (74% relative density). Through characterization of the composite with SEM-EDS mapping, the composite exhibited a uniform mixture of LAGP and PVDF-HFP. The enhancement of the ionic conductivity can be attributed to two factors; the increase in relative density by incorporating polymers, and the formation of an ionic conducting network with the addition of liquid electrolyte. More recently, Clive's group improved the ionic conductivity of the LAGP electrolyte by adding Li-salt (Li-TFSI) into the pellet, resulting in a conductivity of 5×10^{-5} S cm^{-1} at room temperature [91].

Tape-casting of solid-state electrolytes are widely used for solid state battery fabrication. In the past few years, there have been reports on tape-casting of LATP, LAGP, LLZO and sulfide-based electrolytes. The first group of LAT(G)P sheets were developed by Ohara Inc. Using a quenching-crystallization process, which is now commercially available now. However, the LAT(G)P sheets still have room for improvement in terms of performance and thickness before it can be adopted for large scale applications. The tuning of thickness can be achieved by reducing particle size, lowering sintering temperature with sintering additives, and increasing the density by forming composites with epoxy resin [93–95]. Recently, a garnet-type LLZO sheet was prepared by Yi et al., where they used flame-made nano particles to prepare thin LLZO electrolytes. Due to the small grains of LLZO, a highly dense and transparent LLZO thin film was achieved, with a high ionic conductivity of 1.3 mS cm^{-1} [96]. Fu et al. reported a three-dimensional bilayer LLZO sheet where one side of the sheet was porous after the introduction of PMMA polymer as pore-forming agent [97]. This bilayer sheet was mechanically stable and capable of hosting active materials for solid-state batteries. Furthermore, the development of sulfide-electrolytes sheets is critical to realizing high energy density solid-state batteries. Kanno et al. reported the thin film thio-LISICON electrolyte with tape-casting in 2003, however, the ionic conductivity of the sheet-like sulfide electrolyte was largely decreased due to the addition of binder [98]. The binder was left in the electrolyte after processing, and blocked the transportation of lithium ions. Nevertheless, excellent electrochemical performances have been obtained with high conductivity electrolytes in pouch-cell solid-state batteries. In 2017, Nam et al. fabricated a pouch-cell solid state battery with the tape-casting method that was capable of delivering a high energy density with improved safety at high temperature [99].

3.2. Cold sintering of solid-state electrodes

Typically, the sintering temperature of solid electrolytes can reach as high as 700 °C - 1000 °C by conventional sintering processes [1]. Impurity phases were detected at the interface between solid electrolyte and electrode after the high-temperature sintering process, which are capable of blocking the transportation of lithium ions during electrochemical cycling [25]. Thus, the CSP of active materials and solid electrolyte could be a promising route in solving this issue.

In one report by Guo, V_2O_5, a cathode material candidate for lithium-ion batteries, was sintered by a CSP at 120 °C [74,100]. In the TEM micrographs of the CSP, a small amount of amorphous phase was detected at the grain boundaries after the dissolution-precipitation process, which is a typical charac-

teristic for the CSP pellet. To increase the electronic conductivity of the V_2O_5 pellet, 1–2 vol % conductive polymer PEDOT:PSS was added during sintering. It was found that the composite showed an increase in electronic conductivity greater than two orders of magnitude compared to the pure V_2O_5 [100]. Such a composite is possible for application as an electrode in solid-state batteries.

Additionally, the CSP technique was also applied to $LiFePO_4$ cathode materials. A dense pellet consisting of cathode material, active carbon and PVDF was sintered at a low temperature of 240 °C, as shown in Fig. 5 [101]. Instead of using water as the solvent, a LiOH solution was used to increase the solubility of $LiFePO_4$. The density of the electrode was increased gradually with an increase of applied pressure, with a relative density of 85% being achieved at ~750 MPa. After the CSP, the $LiFePO_4$ was found to remain in a pure phase with no visible impurities from XRD characterization. From the cross-section SEM and TEM images, a densified microstructure with the formation of grains with triple points and low porosity was observed, as seen in Fig. 5a. Clean grain boundaries of $LiFePO_4$ with equilibrated dihedral angles occurred at the triple points, where small amounts of amorphous or glassy phases were identified. Cyclic voltammetry of the CSP $LiFePO_4$ electrode exhibited a redox peak around 3.45 V, indicating the lithiation/delithiation in $LiFePO_4$ active materials. In charge-discharge tests, 155 mAh g^{-1} was achieved at 0.1 C during initial discharge process. 340 mAh cm^{-3} was calculated because of the significantly higher density of the electrode in terms of volumetric capacity. Unfortunately, the discharge capacity was still low at high current density.

In a recent paper, the CSP was extended to tape-casted cathode materials, as displayed in Fig. 6 [102]. The sintered electrode was composed of $LiFePO_4$ and carbon nano-fibers, with no additional binder. A high density of 2.42 g cm^{-3} was achieved, corresponding to a relative density of ~70%, which was much higher than conventional tape-casted $LiFePO_4$ electrodes (1.9 g cm^{-3}). Shown in Fig. 6a, the CSP $LiFePO_4$ electrode contains highly-conductive CNF fillers, which are beneficial for electron conduction. Similar to previous reports, some amorphous phase was observed at the grain boundaries in re-

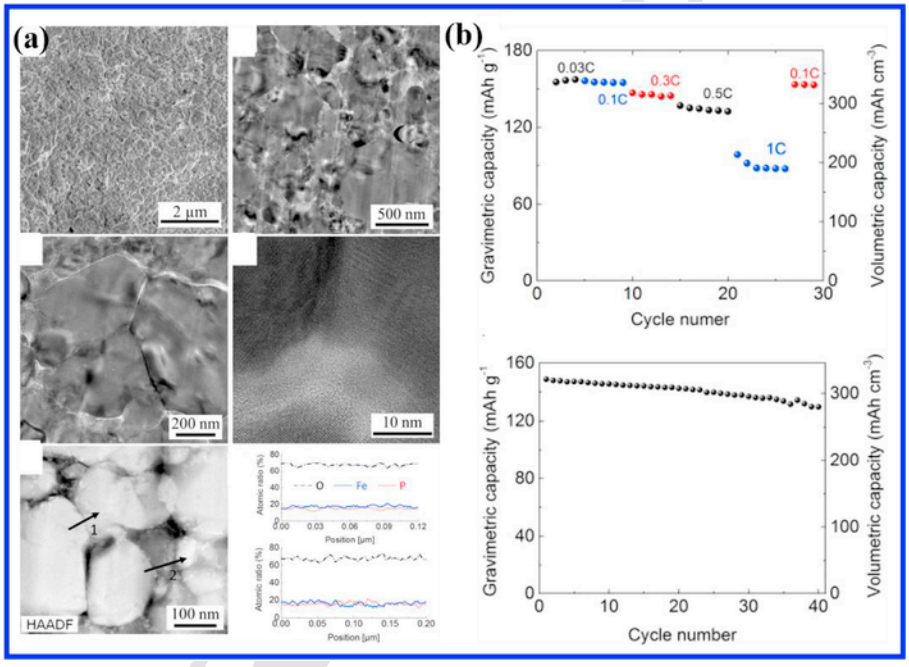

Fig. 5. Cold sintering of a $LiFePO_4$ pellet; (a) TEM images of $LiFePO_4$, and (b) cycling performance of $LiFePO_4$ [101].

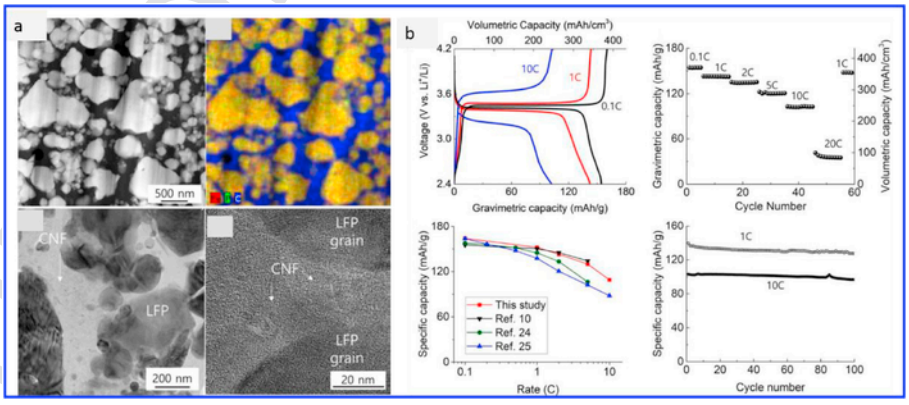

Fig. 6. Cold sintering of $LiFePO_4$/carbon nano-fiber (CNF) thin film, (a) TEM images of $LiFePO_4$/CNF, (b) cycling performance of $LiFePO_4$/CNF [102].

gions of electrode. In the electrochemical tests, the CSP $LiFePO_4$ electrode showed good performance from 0.1 C to 1 C with a volumetric capacity of 373 mAh cm^{-3}. A high volumetric capacity of 247 mAh cm^{-3} and energy capacity of 102 mAh g^{-1} was observed at a rate of 10 C.

4. Conclusion and perspective

In this report, the recent progress in the use of CSP for solid-state electrolytes and electrodes has been summarized. Based on the reported examples, it can be concluded that the CSP is a promising route to obtaining high compact density electrolytes/electrodes. However, the electrochemical properties of the CSP electrolytes/electrodes are still far from real application. There is still a large space for improvement in terms of physical/chemical properties. In addition, detailed characterizations on the microstructure will facilitate the design of high performance electrolyte/electrodes.

Solid electrolytes and electrodes have a long history of manufacturing via thermal sintering. The dense body is achieved through the use of high temperatures to promote mass transport during the sintering process. However, high-temperature sintering invokes the formation of blocking layers due to side-reactions. Thus, the development of new sintering routes at lower temperatures are necessary. Here, a facile sintering technique, the cold sintering process (CSP), is introduced. It enables the densification of electrolyte/electrode at a lower temperature (< 300 °C) in a short period of time. The basic mechanism of the CSP is the dissolution of the sharp-edges of particles by a solvent and subsequent filling of the voids between particles through evaporation of solvent and precipitation of dissolved species. Such an innovative mechanism can render the densification of a broad range of inorganic and inorganic-organic composites. Furthermore, it has been successfully applied in solid-state electrolytes and solid-state batteries with reasonable performance being achieved.

CSP shows great promise in preparation of solid electrolytes and composite electrodes, and needs further exploration. Fundamentally, there are a few issues that need further study:

1. The enhanced ionic conductivity not only arises from the improved density by filling the voids between particles through the precipitation of dissolved species, but also depends on improved bonding between grain boundaries. The following work needs to explore the chemical/physical properties of grain boundaries, such as chemistry, composition, structure and their relationship with improved conductivity, in order to reveal the role of CSP on improving the ionic conductivity.
2. For some target materials, their solubility is low or negligible in liquid solutions, and additives with high solubility and high ionic conductivity are required in order to improve the bonding at grains, tune the space charge layer and enhance the ionic conductivity. In addition, some types of additives may enhance the solubility of target materials in liquid solutions, and need further exploration to widen the application of CSP techniques in solid-state batteries.
3. In composite cathodes, special protection is needed for cathode materials, as most materials may be not chemical stable with liquid solution or are soluble during the CSP. Different surface protection techniques and types of coating materials need to be involved and studied.
4. Cold co-sintering processes between electrolytes and cathodes are necessary in realizing good physical contacts. The

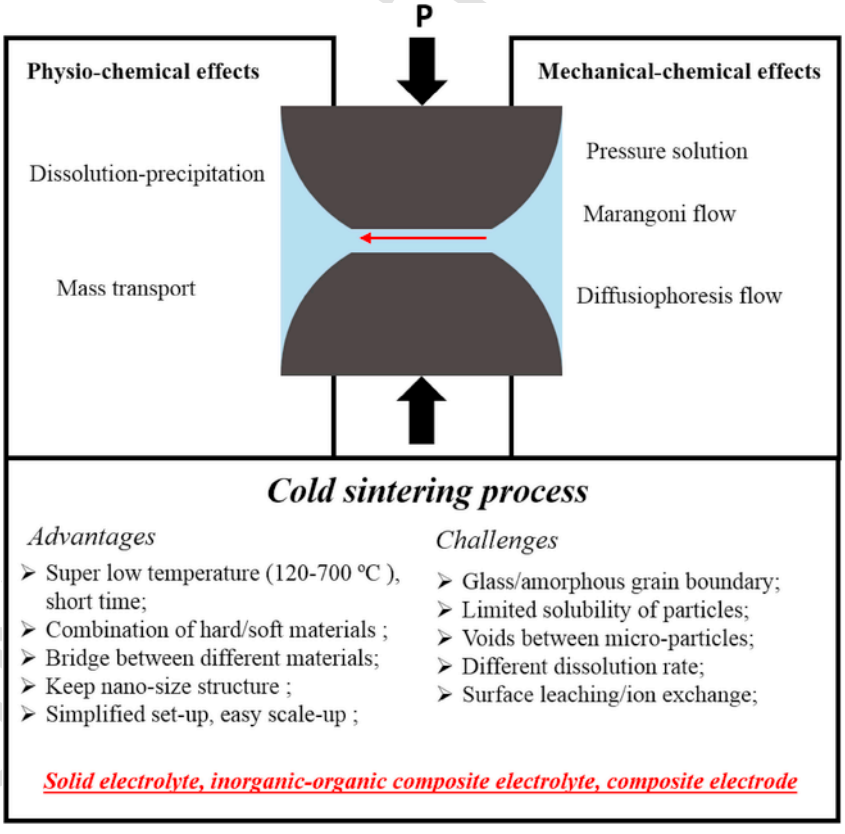

Fig. 7. Summary of Cold sintering process and its application in solid-state batteries.

mismatch between electrolyte and electrode will deteriorate the electrochemical performance of solid-state batteries. By sintering the electrolyte with electrode, a clean and stable interface is beneficial for lithium ion transport.

Although there are many reports in preparing ASSLIBs in coin cells or model-cells, few publication describe attempts to fabricate large-format ASSLIB with scalable production processes, such as wet-coating, screen printing and tape-casting [103]. Cheap materials with low-cost synthesis, processing temperatures, and chemical reactivity are expected to be the main challenges in the scale up stage. The CSP is a low-cost process that can operate at low temperatures, and is a very promising direction in assembling large-format cells. Additionally, the tape-casting process can be incorporated into the CSP process by co-sintering of multilayer materials, suggesting the great potential of scaling-up production [104]. CSP, as an emerging sintering technique, will attract great attentions in the development of solid-state interfaces and solid-state batteries (See Fig. 7).

Uncited references

[30]; [34]; [35].

Acknowledgements

This work was supported by the China Automotive Battery Research Institute-Western University Joint Laboratory, Canada Research Chair (CRC) Program, and Western University.

References

[1] C.W. Sun, J. Liu, Y.D. Gong, D.P. Wilkinson, J.J. Zhang, Nanomater. Energy 33 (2017) 363–386.
[2] W.D. Richards, L.J. Miara, Y. Wang, J.C. Kim, G. Ceder, Chem. Mater. 28 (2016) 266–273.
[3] V. Thangadurai, S. Narayanan, D. Pinzaru, Chem. Soc. Rev. 43 (2014) 4714–4727.
[4] L. Yue, J. Ma, J. Zhang, J. Zhao, S. Dong, Z. Liu, G. Cui, L. Chen, Energy Storage Materials 5 (2016) 139–164.
[5] K. Takada, N. Ohta, L. Zhang, K. Fukuda, I. Sakaguchi, R. Ma, M. Osada, T. Sasaki, Solid State Ionics 179 (2008) 1333–1337.
[6] V. Thangadurai, W. Weppner, Adv. Funct. Mater. 15 (2005) 107–112.
[7] S. Hasegawa, N. Imanishi, T. Zhang, J. Xie, A. Hirano, Y. Takeda, O. Yamamoto, J. Power Sources 189 (2009) 371–377.
[8] D. Liu, W. Zhu, Z. Feng, A. Guerfi, A. Vijh, K. Zaghib, Mater. Sci. Eng., B (2016).
[9] H. Yamane, M. Shibata, Y. Shimane, T. Junke, Y. Seino, S. Adams, K. Minami, A. Hayashi, M. Tatsumisago, Solid State Ionics 178 (2007) 1163–1167.
[10] N. Kamaya, K. Homma, Y. Yamakawa, M. Hirayama, R. Kanno, M. Yonemura, T. Kamiyama, Y. Kato, S. Hama, K. Kawamoto, Nat. Mater. 10 (2011) 682–686.
[11] R. Kanno, M. Murayama, J. Electrochem. Soc. 148 (2001) A742–A746.
[12] S.-T. Kong, H.-J. Deiseroth, J. Maier, V. Nickel, K. Weichert, C. Reiner, Z. Anorg. Allg. Chem. 636 (2010) 1920–1924.
[13] S. Stramare, V. Thangadurai, W. Weppner, Chem. Mater. 15 (2003) 3974–3990.
[14] P. Knauth, Solid State Ionics 180 (2009) 911–916.
[15] M. Matsuo, S.-i. Orimo, Adv. Energy Mater. 1 (2011) 161–172.
[16] C. Cao, Z. Li, X.-L. Wang, X. Zhao, W.-Q. Han, Frontiers in Energy Research 2 (2014).
[17] J.G. Kim, B. Son, S. Mukherjee, N. Schuppert, A. Bates, O. Kwon, M.J. Choi, H.Y. Chung, S. Park, J. Power Sources 282 (2015) 299–322.
[18] J.C. Bachman, S. Muy, A. Grimaud, H.-H. Chang, N. Pour, S.F. Lux, O. Paschos, F. Maglia, S. Lupart, P. Lamp, L. Giordano, Y. Shao-Horn, Chem. Rev. 116 (2016) 140–162.
[19] K. Dokko, K. Hoshina, H. Nakano, K. Kanamura, J. Power Sources 174 (2007) 1100–1103.
[20] J. Xie, N. Imanishi, T. Zhang, A. Hirano, Y. Takeda, O. Yamamoto, J. Power Sources 189 (2009) 365–370.
[21] E. Kobayashi, L.S. Plashnitsa, T. Doi, S. Okada, J.-i. Yamaki, Electrochem. Commun. 12 (2010) 894–896.
[22] P. Hartmann, T. Leichtweiss, M.R. Busche, M. Schneider, M. Reich, J. Sann, P. Adelhelm, J. Janek, J. Phys. Chem. C 117 (2013) 21064–21074.
[23] H. Morimoto, H. Awano, J. Terashima, Y. Shindo, S. Nakanishi, N. Ito, K. Ishikawa, S.-i. Tobishima, J. Power Sources 240 (2013) 636–643.
[24] S. Ohta, T. Kobayashi, T. Asaoka, J. Power Sources 196 (2011) 3342–3345.
[25] K. Park, B.-C. Yu, J.-W. Jung, Y. Li, W. Zhou, H. Gao, S. Son, J.B. Goodenough, Chem. Mater. 28 (2016) 8051–8059.
[26] M. Kotobuki, K. Kanamura, Ceram. Int. 39 (2013) 6481–6487.
[27] S. Ohta, S. Komagata, J. Seki, T. Saeki, S. Morishita, T. Asaoka, J. Power Sources 238 (2013) 53–56.
[28] S. Ohta, J. Seki, Y. Yagi, Y. Kihira, T. Tani, T. Asaoka, J. Power Sources 265 (2014) 40–44.
[29] Y. Li, B. Xu, H. Xu, H. Duan, X. Lü, S. Xin, W. Zhou, L. Xue, G. Fu, A. Manthiram, J.B. Goodenough, Angew. Chem. Int. Ed. 56 (2017) 753–756.
[30] J. Van den Broek, S. Afyon, J.L. Rupp, Adv. Energy Mater. 6 (2016).
[31] F. Han, J. Yue, C. Chen, N. Zhao, X. Fan, Z. Ma, T. Gao, F. Wang, X. Guo, C. Wang, Joule 2 (2018) 497–508.
[32] M. Kotobuki, K. Kanamura, Y. Sato, T. Yoshida, J. Power Sources 196 (2011) 7750–7754.
[33] M. Kotobuki, Y. Suzuki, K. Kanamura, Y. Sato, K. Yamamoto, T. Yoshida, J. Power Sources 196 (2011) 9815–9819.
[34] K. Takada, N. Aotani, S. Kondo, J. Power Sources 43 (1993) 135–141.
[35] K. Iwamoto, N. Aotani, K. Takada, S. Kondo, Solid State Ionics 70 (1994) 658–661.
[36] N. Ohta, K. Takada, I. Sakaguchi, L. Zhang, R. Ma, K. Fukuda, M. Osada, T. Sasaki, Electrochem. Commun. 9 (2007) 1486–1490.
[37] T. Kobayashi, A. Yamada, R. Kanno, Electrochim. Acta 53 (2008) 5045–5050.
[38] S. Yubuchi, A. Hayashi, M. Tatsumisago, Meeting Abstracts, The Electrochemical Society, 2016, 3982–3982.
[39] Y. Kato, S. Hori, T. Saito, K. Suzuki, M. Hirayama, A. Mitsui, M. Yonemura, H. Iba, R. Kanno, Nat. Energy 1 (2016) 16030.
[40] D. Sohrabi Baba Heidary, M. Lanagan, C.A. Randall, J. Eur. Ceram. Soc. (2017).
[41] K. Naik, University of Trento, 2014, Italy.
[42] S. Berbano, The Pennsylvania State University, 2017.
[43] E. Rangasamy, J. Wolfenstine, J. Sakamoto, Solid State Ionics 206 (2012) 28–32.
[44] J.L. Allen, J. Wolfenstine, E. Rangasamy, J. Sakamoto, J. Power Sources 206 (2012) 315–319.
[45] A. Sakuda, A. Hayashi, M. Tatsumisago, Sci. Rep. 3 (2013) 2261.
[46] R. Chaim, M. Levin, A. Shlayer, C. Estournes, Adv. Appl. Ceram. 107 (2013) 159–169.
[47] R. Muccillo, E.N.S. Muccillo, J. Eur. Ceram. Soc. 33 (2013) 515–520.
[48] Y. Zhang, F. Chen, R. Tu, Q. Shen, L. Zhang, J. Power Sources 268 (2014) 960–964.
[49] Y. Zhang, J. Cai, F. Chen, R. Tu, Q. Shen, X. Zhang, L. Zhang, J. Alloy. Comp. 644 (2015) 793–798.
[50] A. Rosenberger, Y. Gao, L. Stanciu, Solid State Ionics 278 (2015) 217–221.
[51] E.C. Bucharsky, K.G. Schell, A. Hintennach, M.J. Hoffmann, Solid State Ionics 274 (2015) 77–82.
[52] M. Cologna, A.L.G. Prette, R. Raj, J. Am. Ceram. Soc. 94 (2011) 316–319.
[53] I. Lisenker, C.R. Stoldt, Frontiers in Energy Research 4 (2016).
[54] J. Wang, X.-P. Jiang, X.-L. Wei, H. Yang, X.-D. Shen, J. Alloy. Comp. 497 (2010) 295–299.
[55] H.X. Geng, A. Mei, C. Dong, Y.H. Lin, C.W. Nan, J. Alloy. Comp. 481 (2009) 555–558.
[56] W. Chen, U. Anselmi-Tamburini, J.E. Garay, J.R. Groza, Z.A. Munir, Mater. Sci. Eng. 394 (2005) 132–138.
[57] M. Nygren, Z. Shen, Solid State Sci. 5 (2003) 125–131.
[58] Y. Li, M. Liu, K. Liu, C.-A. Wang, J. Power Sources 240 (2013) 50–53.
[59] S.-W. Baek, J.-M. Lee, T.Y. Kim, M.-S. Song, Y. Park, J. Power Sources 249 (2014) 197–206.
[60] K. Chen, Y. Shen, Y. Zhang, Y. Lin, C.-W. Nan, J. Power Sources 249 (2014) 306–310.
[61] A. Kubanska, L. Castro, L. Tortet, O. Schäf, M. Dollé, R. Bouchet, Solid State Ionics 266 (2014) 44–50.

[62] A. Aboulaich, R. Bouchet, G. Delaizir, V. Seznec, L. Tortet, M. Morcrette, P. Rozier, J.M. Tarascon, V. Viallet, M. Dollé, Adv. Energy Mater. 1 (2011) 179–183.
[63] E. Dumont-Botto, C. Bourbon, S. Patoux, P. Rozier, M. Dolle, J. Power Sources 196 (2011) 2274–2278.
[64] T. Okumura, T. Takeuchi, H. Kobayashi, Meeting Abstracts, 20161066, MA2016-03.
[65] G. Delaizir, V. Viallet, A. Aboulaich, R. Bouchet, L. Tortet, V. Seznec, M. Morcrette, J.M. Tarascon, P. Rozier, M. Dollé, Adv. Funct. Mater. 22 (2012) 2140–2147.
[66] T. Okumura, T. Takeuchi, H. Kobayashi, Solid State Ionics 288 (2016) 248–252.
[67] T. Okumura, T. Takeuchi, H. Kobayashi, J. Ceram. Soc. Jpn. 125 (2017) 276–280.
[68] E. Gutmanas, A. Rabinkin, M. Roitberg, Scripta Metall. 13 (1979) 11–15.
[69] N. Yamasaki, K. Yanagisawa, M. Nishioka, S. Kanahara, J. Mater. Sci. Lett. 5 (1986) 355–356.
[70] A. Ndayishimiye, A. Largeteau, M. Prakasam, S. Pechev, M.-A. Dourges, G. Goglio, Scripta Mater. 145 (2018) 118–121.
[71] A. Ndayishimiye, A. Largeteau, S. Mornet, M. Duttine, M.-A. Dourges, D. Denux, M. Verdier, M. Gouné, T. Hérisson de Beauvoir, C. Elissalde, G. Goglio, J. Eur. Ceram. Soc. 38 (2018) 1860–1870.
[72] C. Vakifahmetoglu, J.F. Anger, V. Atakan, S. Quinn, S. Gupta, Q. Li, L. Tang, R.E. Riman, J. Am. Ceram. Soc. 99 (2016) 3893–3901.
[73] H. Guo, J. Guo, A. Baker, C.A. Randall, ACS Appl. Mater. Interfaces 8 (2016) 20909–20915.
[74] J. Guo, S.S. Berbano, H. Guo, A.L. Baker, M.T. Lanagan, C.A. Randall, Adv. Funct. Mater. 26 (2016) 7115–7121.
[75] J. Guo, H. Guo, A.L. Baker, M.T. Lanagan, E.R. Kupp, G.L. Messing, C.A. Randall, Angew Chem. Int. Ed. Engl. 55 (2016) 11457–11461.
[76] H. Guo, A. Baker, J. Guo, C.A. Randall, D. Johnson, J. Am. Ceram. Soc. 99 (2016) 3489–3507.
[77] H. Guo, J. Guo, A. Baker, C.A. Randall, J. Am. Ceram. Soc. 100 (2017) 491–495.
[78] J. Guo, A.L. Baker, H. Guo, M. Lanagan, C.A. Randall, J. Am. Ceram. Soc. 100 (2017) 669–677.
[79] J.-P. Maria, X. Kang, R.D. Floyd, E.C. Dickey, H. Guo, J. Guo, A. Baker, S. Funihashi, C.A. Randall, J. Mater. Res. (2017) 1–14.
[80] C.A. Randall, J. Guo, A. Baker, M. Lanagan, H. Guo, in, Google Patents, 2017.
[81] H. Guo, A. Baker, J. Guo, C.A. Randall, ACS Nano 10 (2016) 10606–10614.
[82] H. Guo, T.J.M. Bayer, J. Guo, A. Baker, C.A. Randall, J. Eur. Ceram. Soc. 37 (2017) 2303–2308.
[83] I.J. Induja, M.T. Sebastian, Mater. Lett. 211 (2018) 55–57.
[84] J. Gonzalez-Julian, K. Neuhaus, M. Bernemann, J. Pereira da Silva, A. Laptev, M. Bram, O. Guillon, Acta Mater. 144 (2018) 116–128.
[85] J. Nie, Y. Zhang, J.M. Chan, R. Huang, J. Luo, Scripta Mater. 142 (2018) 79–82.
[86] W.B. Hong, L. Li, M. Cao, X.M. Chen, J. Am. Ceram. Soc..
[87] A. Sakuda, A. Hayashi, M. Tatsumisago, Current Opinion in Electrochemistry 6 (2017) 108–114.
[88] A. Sakuda, A. Hayashi, Y. Takigawa, K. Higashi, M. Tatsumisago, J. Ceram. Soc. Jpn. 121 (2013) 946–949.
[89] M. Tatsumisago, R. Takano, M. Nose, K. Nagao, A. Kato, A. Sakuda, K. Tadanaga, A. Hayashi, J. Ceram. Soc. Jpn. 125 (2017) 433–437.
[90] K. Nagao, M. Nose, A. Kato, A. Sakuda, A. Hayashi, M. Tatsumisago, Solid State Ionics 308 (2017) 68–76.
[91] W. Lee, C. Lyon, C. Ranall, E. Gomez, MRS Fall Meeting, 2017.
[92] S.S. Berbano, J. Guo, H. Guo, M.T. Lanagan, C.A. Randall, J. Am. Ceram. Soc. 100 (2017) 2123–2135.
[93] L. Puech, C. Cantau, P. Vinatier, G. Toussaint, P. Stevens, J. Power Sources 214 (2012) 330–336.
[94] M. Zhang, K. Takahashi, I. Uechi, Y. Takeda, O. Yamamoto, D. Im, D.-J. Lee, B. Chi, J. Pu, J. Li, N. Imanishi, J. Power Sources 235 (2013) 117–121.
[95] M. Zhang, Z. Huang, J. Cheng, O. Yamamoto, N. Imanishi, B. Chi, J. Pu, J. Li, J. Alloy. Comp. 590 (2014) 147–152.
[96] E. Yi, W. Wang, J. Kieffer, R.M. Laine, J. Mater. Chem. 4 (2016) 12947–12954.
[97] K.K. Fu, Y. Gong, G.T. Hitz, D.W. McOwen, Y. Li, S. Xu, Y. Wen, L. Zhang, C. Wang, G. Pastel, Energy Environ. Sci. 10 (2017) 1568–1575.
[98] T. Inada, K. Takada, A. Kajiyama, M. Kouguchi, H. Sasaki, S. Kondo, M. Watanabe, M. Murayama, R. Kanno, Solid State Ionics 158 (2003) 275–280.
[99] Y.J. Nam, D.Y. Oh, S.H. Jung, Y.S. Jung, J. Power Sources 375 (2018) 93–101.
[100] J. Guo, H. Guo, D.S.B. Heidary, S. Funahashi, C.A. Randall, J. Eur. Ceram. Soc. 37 (2017) 1529–1534.
[101] J.-H. Seo, J. Guo, H. Guo, K. Verlinde, D.S.B. Heidary, R. Rajagopalan, C.A. Randall, Ceram. Int. 43 (2017) 15370–15374.
[102] J.-H. Seo, K. Verlinde, J. Guo, D.S.B. Heidary, R. Rajagopalan, T.E. Mallouk, C.A. Randall, Scripta Mater. 146 (2018) 267–271.
[103] J. Schnell, T. Günther, T. Knoche, C. Vieider, L. Köhler, A. Just, M. Keller, S. Passerini, G. Reinhart, J. Power Sources 382 (2018) 160–175.
[104] S. Funahashi, H. Guo, J. Guo, A.L. Baker, K. Wang, K. Shiratsuyu, C.A. Randall, J. Am. Ceram. Soc. 100 (2017) 3488–3496.